Hindawi Publishing Corporation
International Journal of Photoenergy
Volume 2011, Article ID 532578, 14 pages
doi:10.1155/2011/532578

Research Article

TiO_2/ZnS/CdS Nanocomposite for Hydrogen Evolution and Orange II Dye Degradation

Václav Štengl and Daniela Králová

Department of Solid State Chemistry, Institute of Inorganic Chemistry AS CR, v.v.i., 250 68 Řež, Czech Republic

Correspondence should be addressed to Václav Štengl, stengl@iic.cas.cz

Received 18 January 2011; Revised 14 April 2011; Accepted 21 May 2011

Academic Editor: Panagiotis Lianos

TiO_2/ZnS/CdS composites for photocatalytic hydrogen production from water were prepared by homogeneous hydrolysis of aqueous solutions mixture of $TiOSO_4$, $ZnSO_4$, and $CdSO_4$ with thioacetamide. Hydrogen evolution was observed in the presence of palladium and platinum nanoparticles deposited on TiO_2/ZnS/CdS composites. The morphology was obtained by scanning electron microscopy, the nitrogen adsorption-desorption was used for determination of surface area (BET) and porosity. The method of UV-VIS diffuse reflectance spectroscopy was employed to estimate band-gap energies of prepared TiO_2/ZnS/CdS nanocomposites. The photocatalytic activity of the prepared samples were assessed by photocatalytic decomposition of Orange II dye in an aqueous slurry under UV irradiation at 365 nm wavelength and visible light up to 400 nm wavelength. Doped titanium dioxide by the CdS increased band-gap energy and doping with ZnS increased photocatalytic activity. The best photocatalytic activity for H_2 evolution shows sample named TiZnCd7 on surface deposited with palladium, which contains 20.21% TiO_2, 78.5% ZnS, and 1.29% CdS.

1. Introduction

Nano-sized TiO_2 photocatalytic water-splitting technology has great potential for low-cost and environmentally friendly solar-hydrogen production to support the future hydrogen economy [1]. Semiconductor photocatalysis (TiO_2, ZnO) has been intensively studied in recent decades for a wide variety of application such as hydrogen production from water splitting and water and air treatment. Nevertheless, the majority of photocatalysts are, however, wide band-gap semiconductors which are active only under UV irradiation. On the other hand, in order to effectively utilize visible solar radiation, the present work investigates various types of visible-light active photocatalysts including metal ion-doped TiO_2, nanocomposites of TiO_2 and ZnS or CdS, and a mixed-phase ZnS-CdS matrix interlinked with elemental Pt deposits.

The vast majority of today's researches are focused on TiO_2 thin films that have been synthesized by radio-frequency magnetron sputtering and/or sol-gel method to study the hydrogen generation by photocatalytic water splitting under visible light irradiation. It is necessary to mention that there is quite a long time period to obtain the constant H_2 generation on such TiO_2 films. This phenomena both because of the separated evolution of H_2 and O_2 gases, and consequently thanks to the back-reaction effect [2]. Following the work of authors using different approaches to resolve some or all of the disadvantages H_2 production by using TiO_2 films, Cr or Fe ion-doped TiO_2 thin films have been synthesized by radio-frequency magnetron sputtering and a sol-gel method to study hydrogen generation by photocatalytic water splitting under visible light irradiation. The doping method, dopant concentration, charge transfer from metal dopants to TiO_2, and type of dopants used for modification of TiO_2 were investigated for their ability to enhance photocatalytic activity [3].

Highly dispersed iridium and cobalt metal particles (average 3 nm) were introduced in the texture of the synthesized titania nanotube by ion-exchange method, which were found to be effective photocatalysts for the production of stoichiometric hydrogen and oxygen by the splitting of water under the visible light irradiation [4].

Fe^{3+}-doped titania photocatalysts were prepared by hydrothermal treatment for the photocatalytic water splitting to produce stoichiometric hydrogen and oxygen under visible light irradiation [5]. Sensitized photocatalytic production of hydrogen from water splitting is investigated under visible light irradiation over mesoporous-assembled titanium dioxide nanocrystal photocatalysts, without and with Pt loading [6]. ZnO-CdS core-shell nanorods with a wide absorption range were designed and synthesized by a two-step route. The ZnO-CdS core-shell nanorods exhibit stable and high photocatalytic activity for water splitting into hydrogen in the presence of S^{2-} and $SO_3{}^{2-}$ as sacrificial reagents [7].

Mixed semiconductor CdS-ZnS-TiO_2 (1 : 1 : 1) mixture system over different supports like MgO, CaO, γ-Al_2O_3, SiO_2, and modified MgO and CaO have been prepared, characterized and tested for H_2 production in a $S^{2-}/SO_3{}^{2-}$ mixture solution [8]. In order to efficiently use the UV-vis light in the photocatalytic reaction, a novel (CdS/ZnS)/Ag_2S + RuO_2/TiO_2 was synthesized by chemical coprecipitation and metal ion implantation, and this composite exhibited much higher photocatalytic activity for the generation of hydrogen [9]. Powdered and immobilized Pt/CdS/TiO_2 photocatalysts were used to oxidize model inorganic ($S^{2-}/SO_3{}^{2-}$) and organic (ethanol) sacrificial agents-pollutants in water. Powdered Pt/CdS/TiO_2 photocatalysts of variable CdS content (0–100%) were synthesized by precipitation of CdS nanoparticles on TiO_2 (Degussa P25) followed by deposition of Pt (0.5 wt%) [10].

As it has been shown earlier [11] the homogeneous precipitation with urea leads to anatase nanoparticles assembled into rather big (1-2 μm) porous clusters consist of small 4-5 nm crystallites embodied good photocatalytic properties. For substitution of urea, we used the modified homogeneous precipitation with thioacetamide to prepare TiO_2/ZnS/CdS nanocomposites. In the same way as the urea method, the homogeneous precipitation of metal sulphides by thermal decomposition of thioacetamide (TAA) can be used [12]. Thioacetamide at temperature higher than 60°C in acidic solution released hydrogen sulphide:

$$CH_3CSNH_2 + H_2O \longrightarrow CH_3CONH_2 + H_2S \quad (1)$$

$$H_2S + H_2O \longrightarrow HS^- + H_3O^+ \quad (2)$$

$$Zn^{2+} + HS^- \longrightarrow ZnS \quad (3)$$

$$Cd^{2+} + HS^- \longrightarrow CdS. \quad (4)$$

The reaction of products are nanosized spherical particles [13] with a well-developed microstructure, but different from homogeneous urea precipitation. These products have high specific surface area and are properly washed and filtered. In the reaction conditions, the spherical agglomerates of titania are formed by thermal hydrolysis of titanyl sulphate [14] and agglutinated with spherical agglomerates of ZnS and CdS, respectively, precipitated with thioacetamide. As-prepared TiO_2/ZnS/CdS nanocomposites by homogeneous hydrolysis with thioacetamide exhibited new optical properties concerning the absorption, which were different from those of the bulk anatase [15], CdS [16], or sphalerite [17].

Table 1: Reaction conditions of nanocomposites TiO_2/ZnS/CdS.

Sample	$TiOSO_4$(g)	$ZnSO_4$ (g)	$CdSO_4$(g)	TAA (g)
TiZnCd1	100	100	10	50
TiZnCd2	100	50	10	50
TiZnCd3	100	100	5	50
TiZnCd4	100	50	5	50
TiZnCd5	100	100	1	50
TiZnCd6	100	50	1	50
TiZnCd7	50	100	1	50
TiZnCd8	50	100	5	50
TiZnCd9	50	100	10	50
TiZnCd10	50	50	50	50

During our study, ten samples were synthesized, labeled as TiZnCd1–TiZnCd10. As a preparation method, was select homogeneous hydrolysis of titania, zinc, and cadmium sulphates with thioacetamide (TAA). The photocatalytic activity of TiO_2/ZnS/CdS nanocomposites was assessed by the photocatalytic decomposition of Orange II dye in an aqueous slurry under irradiation of 365 nm and up to 400 nm wavelength. Subsequently, the above prepared samples were deposited by noble metal palladium and/or platinum nanoparticles. And as such they were used for the photocatalytic hydrogen evolution.

2. Experimental

2.1. Synthesis of ZnS and CdS Doped Titania. All used chemicals, titanium oxosulphate ($TiOSO_4$), zinc(II) sulphate ($ZnSO_4 \cdot 7H_2O$), cadmium(II) sulphate ($CdSO_4 \cdot 8/3H_2O$), sodium borohydride ($NaBH_4$), and thioacetamide (TAA), were of analytical grade and were supplied by Aldrich. The noble metal, palladium, platinum, gold, silver, iridium, rhenium, and ruthenium as standard solution for atomic absorption spectroscopy (AAS, 1000 mg/L, TraceCERT) were obtained from Fluka.

Titanium oxosulphate, zinc(II) sulphate, and cadmium(II) sulphate were dissolved in 4 L of distilled water and 50 g of TAA was added (see Table 1). The reaction mixture was adjusted to pH = 2 with sulphuric acid. The reaction mixture was heated at the temperature of 80°C under stirring for 4 hours. The thus synthesized TiO_2/ZnS/CdS samples were washed with distilled water with decantation, filtered off, and dried at 105°C in a drying kiln. Using with this method ten samples labeled TiZnCd1–TiZnCd10 were prepared.

2.2. Noble Metal Deposition. 1 g photocatalyst (prepared TiO_2/ZnS/CdS or P25) was sonicated 30 min in 100 mL of water in ultrasonic bath (300 W, 35 kHz) and added 1 mL of noble metal 1000 mg L^{-1} AAS solution. The reaction mixture was mixed on a magnetic stirrer and very slowly the 0.001 M solution of sodium borohydride was added. The formation of

Me^0 was monitored using UV-VIS spectrophotometer. The noble metal AAS solution shows an intense characteristic absorption band in UV region at 296 nm of Pd^{3+} and Pt^{4+} ions, at 300 nm for Cu^{2+} and Ag^+ ions, 315 nm for Au^{3+} ion, in visible region at 450 nm of Ru^{3+} ion, and 488 nm of Ir^{3+} ion. Noble metal deposition on the surface of photocatalyst was monitored by disappearance of these intense absorption band.

Obtained suspension of photocatalyst (Degussa P25) with noble metals (Pt, Pd, Ru—light grey powder, Au—light purple powder, Ag—light brown purple powder, Ir, Rh, Cu—slightly yellow powder) deposition were centrifuged and washed in water.

2.3. Characterization Methods. Diffraction patterns were collected with diffractometer PANalytical X'Pert Pro equipped with conventional X-ray tube (Cu K_α radiation, 40 kV, 30 mA) and a linear position sensitive detector PIXcel with an antiscatter shield. A programmable divergence slit set to a fixed value of 0.5 deg, Soller slits of 0.02 rad, and mask of 15 mm were used in the primary beam. A programmable antiscatter slit set to fixed value of 0.5 deg., Soller slit of 0.02 rad, and Niβ-filter were used in the diffracted beam. Qualitative analysis was performed with the DiffracPlus Eva software package (Bruker AXS, Germany) using the JCPDS PDF-2 database [18]. For quantitative analysis of XRD patterns we used Diffrac-Plus Topas (Bruker AXS, Germany, version 4.1) with structural models based on ICSD database [19]. This program permits to estimate the weight fractions of crystalline phases and mean coherence length by means of Rietveld refinement procedure.

Scanning electron microscopy (FESEM) was performed with a high-resolution, field-emission gun SEM microscope Quanta 200 FEG (FEI, Czech Republic) equipped with an energy dispersive X-ray spectrometer (EDS); specimens for morphological investigations were prepared by evaporation of a droplet of samples dispersion on a carbon support. The specimens were then imaged in the low-vacuum mode using accelerating voltages of 30 kV.

The surface areas of samples were determined from nitrogen adsorption-desorption isotherms at liquid nitrogen temperature using a Coulter SA3100 instrument with outgas 15 min at 150°C. The Brunauer-Emmett-Teller (BET) method was used for surface area calculation [20], the pore size distribution (pore diameter, pore volume, and micropore surface area of the samples) was determined by the Barrett-Joyner-Halenda (BJH) method [21].

Diffuse reflectance UV/VIS spectra for evaluation of photophysical properties were recorded in the diffuse reflectance mode (R) and transformed to absorption spectra through the Kubelka-Munk function [22]. A Perkin Elmer Lambda 35 spectrometer equipped with a Labsphere RSAPE-20 integration sphere with $BaSO_4$ as a standard was used.

Photocatalytic activity of samples was assessed from the kinetics of the photocatalytic degradation of 0.02 M Orange II dye (sodium salt 4-[(2-hydroxy-1-naphtenyl)azo]-benzene-sulfonic acid) in aqueous slurries. The azo-dyes (Orange II, Methyl Red, Congo Red, etc.) are not absorbed on titania surfaces in contrast to methylene blue. For azo-dye degradation, the complete mass balance in nitrogen indicated that the central –N=N– azo-group was converted in gaseous dinitrogen, which is ideal for the elimination of nitrogen-containing pollutants, not only for environmental photocatalysis but also for any physicochemical method [23]. Direct photolysis employing artificial UV light or solar energy source cannot mineralize Orange II [24]. Kinetics of the photocatalytic degradation of aqueous Orange II dye solution was measured by using a self-constructed photoreactor [25]. The photoreactor consists of a stainless steel cover and quartz tube with fluorescent lamp Narva with power 13 W and light intensity ~3.5 mW cm^{-2}. Black light (365 nm) for UV and warmwhite (upon 400 nm) for visible light irradiation were used. Orange II dye solution was circulated by means of membrane pump through flow cuvette. The concentration of Orange II dye was determined by measuring absorbance at 480 nm with VIS spectrophotometer ColorQuestXE. The 0.5 g of titania sample was sonicated for 10 min with a ultrasonic bath (300 W, 35 kHz) before use. The pH of the resulting suspension was taken as the initial value for neutral conditions and under the experiment was kept at value 7.0.

2.4. Photocatalytic H_2 Production. Photocatalytic H_2 production reaction was carried out in a self-constructed quartz batch photocatalytic reactor with closed gas-circulation system (see Figure 1). The photocatalyst (1 g) was suspended in distilled water by means of magnetic stirrer within an inner irradiation-type reactor. A high-pressure Hg lamp (400 W) was utilized as the light source. Prior to the reaction, the mixture was deaerated by purging with Ar gas repeatedly. For H_2 measurement the Xgard Type 6 gas detector from firm CROWCON was used. The gas detector measure in range 0–10 vol% H_2 in air on current output ~4–20 mA. The calibration curve of output current of hydrogen sensor is shown in Figure 2. The measured values were recalculated to concentration c (vol%) $= I * R_m/I_{sat} - I_0$ where I is current of detector, I_{sat} is current of detector in the saturated state, I_0 is current of detector at zero concentration of hydrogen, and R_m is maximum range of detector. The basic measurements and calibrations of the apparatus for photocatalytic H_2 evolution were made in the commercial photocatalyst P25 with deposition of Pt, Pd, Ru, Au, Ag, Ir, Rh, and Cu. The evolution of hydrogen was achieved only in samples P25 with surface deposition of platinum, palladium, and gold (see Figure 3.). P25 after deposition of other noble metals (Ru, Ag, Ir, Rh, and Cu) showed no effect of hydrogen evolution and therefore for deposition of TiZnSCdS composites only Pt, Pd, and Au were used. However, samples TiZnSCdS deposited with the Au also showed no effect of hydrogen evolution.

3. Results and Discussion

The powder XRD patterns of the TiO_2/ZnS/CdS composite prepared by homogeneous hydrolysis of $TiOSO_4$ and Zn and Cd sulphates with thioacetamide are shown in Figures 4 and 5, the phase composition and crystallite size are presented in Table 2. According to SEM the prepared nanocomposites are a physical mixture of anatase, Zn, and Cd sulphides,

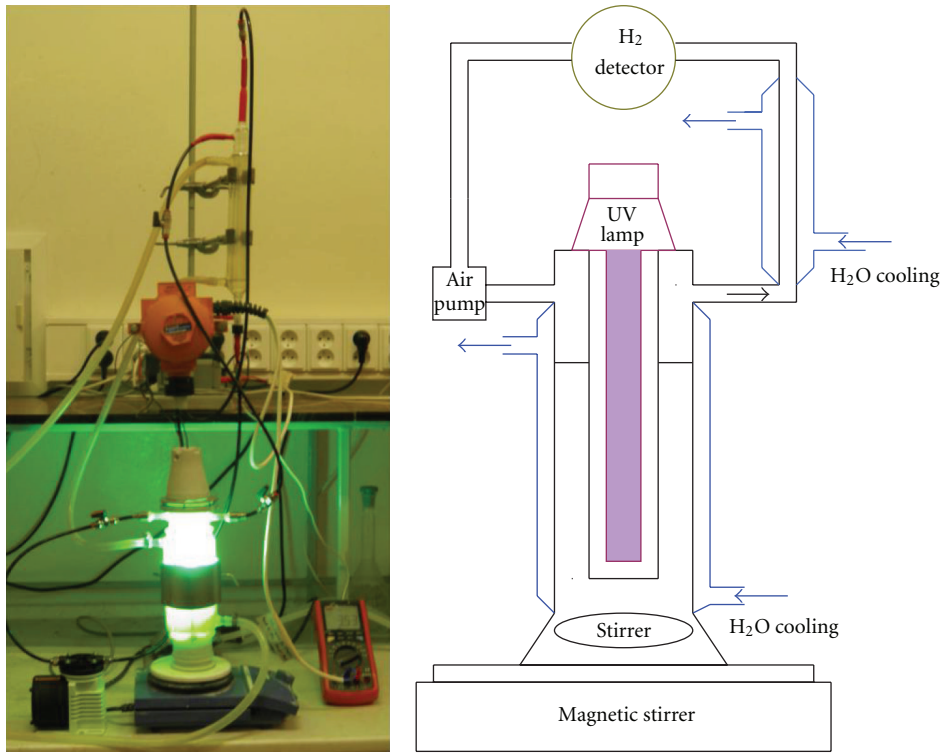

Figure 1: Batch photocatalytic reactor for H_2 evolution.

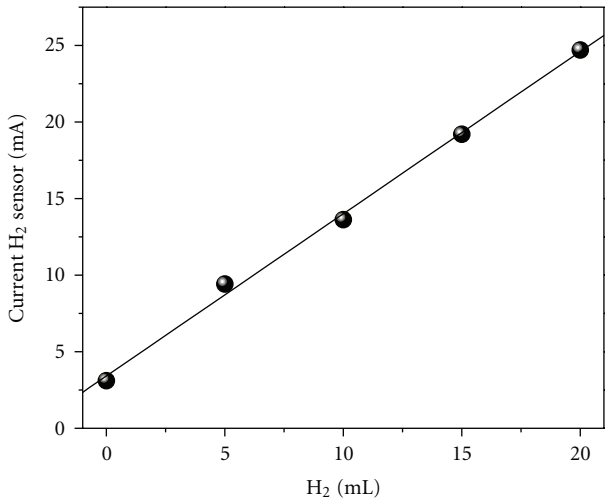

Figure 2: Calibration curve of H_2 detector.

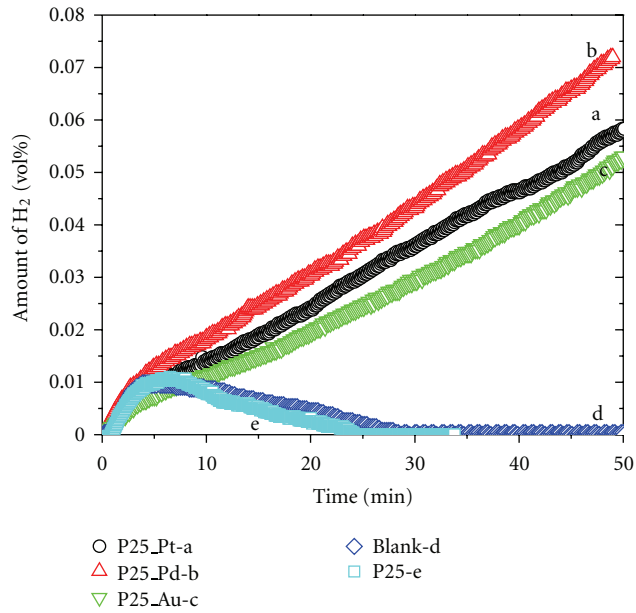

Figure 3: H_2 evolution on Pd, Pt, and Au deposited Degussa P25, pure Degussa P25, and pure water without catalyst (blank).

particle sizes are only a few micrometers, and hence Rietveld refinement can be safely used for quantitative phase analysis. From the XRD patterns and the corresponding characteristic 2Θ values of the diffraction peaks, it can be confirmed that TiO_2 in as-prepared samples is identified as anatase-phase (ICDD PDF 21-1272) while the ZnS is sphalerite-phase (ICDD PDF 5-0566) and CdS is hawleyite-phase (ICDD PDF 10-0454). No other polymorph of titania are observed.

The average size t of crystallites was calculated from the peak half-width B, using the Scherrer equation [26],

$$t = \frac{k\lambda}{B\cos\Theta}, \tag{5}$$

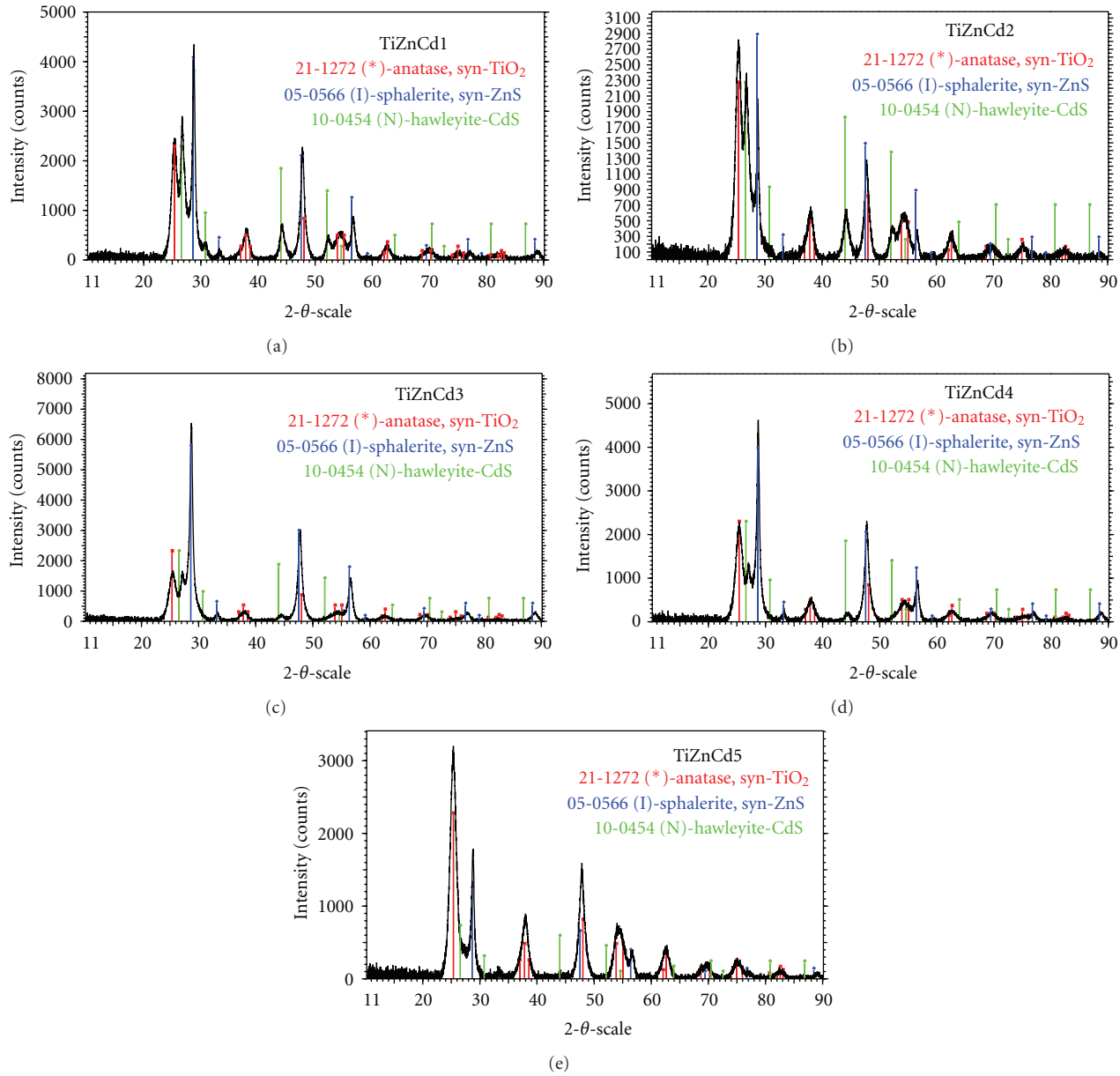

Figure 4: XRD patterns of sample (a) TiZnCd1, (b) TiZnCd2, (c) TiZnCd3, (d) TiZnCd4, and (e) TiZnCd5.

where k is a shape factor of the particle (it is 1 if the spherical shape is assumed) and λ and Θ are the wavelength and the incident angle of the X-rays, respectively. The peak width was measured at half of the maximum intensity. The crystallite size was calculated from diffraction plane (1 0 1) of anatase, diffraction plane (1 1 1) of sphalerite, and diffraction plane (1 1 1) of hawleyite. The relative amount of anatase, sphalerite, and hawleyite phase was calculated from XRD patterns by Diffrac-Plus Topas v.4.1.

The solid solutions of $Cd_{1-x}Zn_xS$, respectively, $Zn_{1-x}Cd_xS$ may arise under hydrothermal conditions [27], at temperature range 150–700°C [28] or under microwave irradiation [29]. The X-ray diffraction lines show no distinct shift that suggests the creation of solid solution $Cd_{1-x}Zn_xS$ [30].

The specific surface area of the samples, calculated by the multipoint Brunauer-Emmett-Teller (BET) method and total pore volume, micropore surface area, and micropore volume are listed in Table 3. For the all samples, the isotherm of a type IV isotherm characteristic of mesoporous material with type H2 hysteresis is typical, which is a characteristic of mesoporous materials and can be ascribed to capillary condensation in mesopores (see Figure 6). The size of mesopores is on the border with micropores, corresponding to size of ~3-4 nm. According de Bore's characterization [31], all samples have characteristic of Type E hysteresis loop. This hysteresis type is connected with ink-bottle pores or with interconnected capillaries. All samples have a microporous surface area in interval 5–40 $m^2 g^{-1}$.

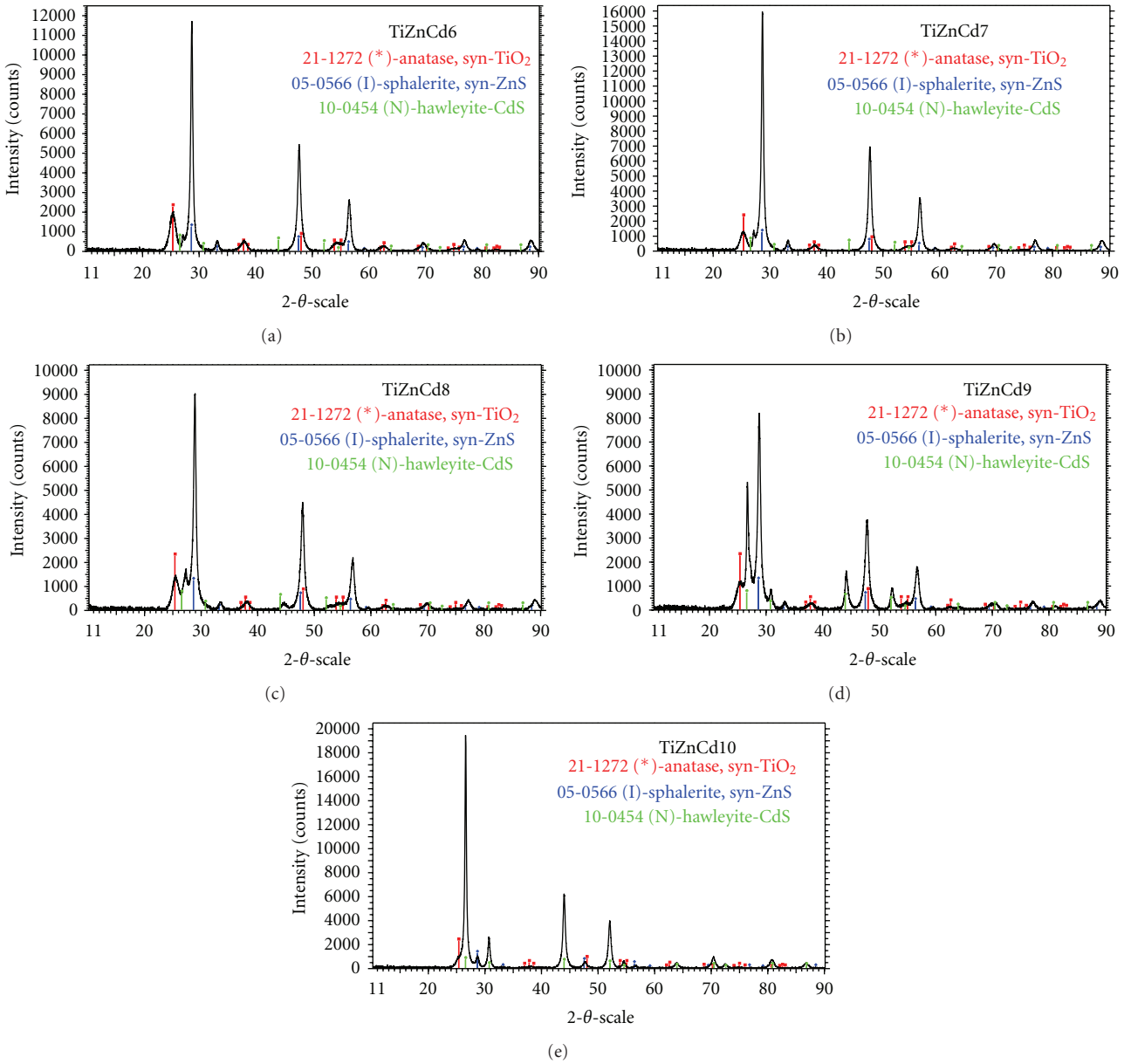

Figure 5: XRD patterns of sample (a) TiZnCd6, (b) TiZnCd7, (c) TiZnCd8, (d) TiZnCd9, and (e) TiZnCd10.

Table 2: Phase composition and crystallite size of nanocomposites TiO_2/ZnS/CdS.

Sample	Anatase (%)	Anatase (nm)	Sphalerite (%)	Sphalerite (nm)	Hawleyite (%)	Hawleyite (nm)
TiZnCd1	59.54	15.7	28.78	21.5	11.68	15.0
TiZnCd2	77.98	15.2	11.5	21.1	10.97	11.5
TiZnCd3	39.88	9.7	56.5	20.5	3.61	13.5
TiZnCd4	62.46	12.0	34.92	20.5	2.62	19.8
TiZnCd5	86.61	15.0	12.71	21.1	0.68	6.9
TiZnCd6	37.44	15.2	61.51	26.2	1.05	6.3
TiZnCd7	20.21	12.5	78.5	28.7	1.29	6.1
TiZnCd8	28.29	13.0	66.31	23.8	5.40	14.3
TiZnCd9	27.49	9.2	57.86	22.4	14.66	23.5
TiZnCd10	7.82	33.4	6.86	23.7	85.32	31.8

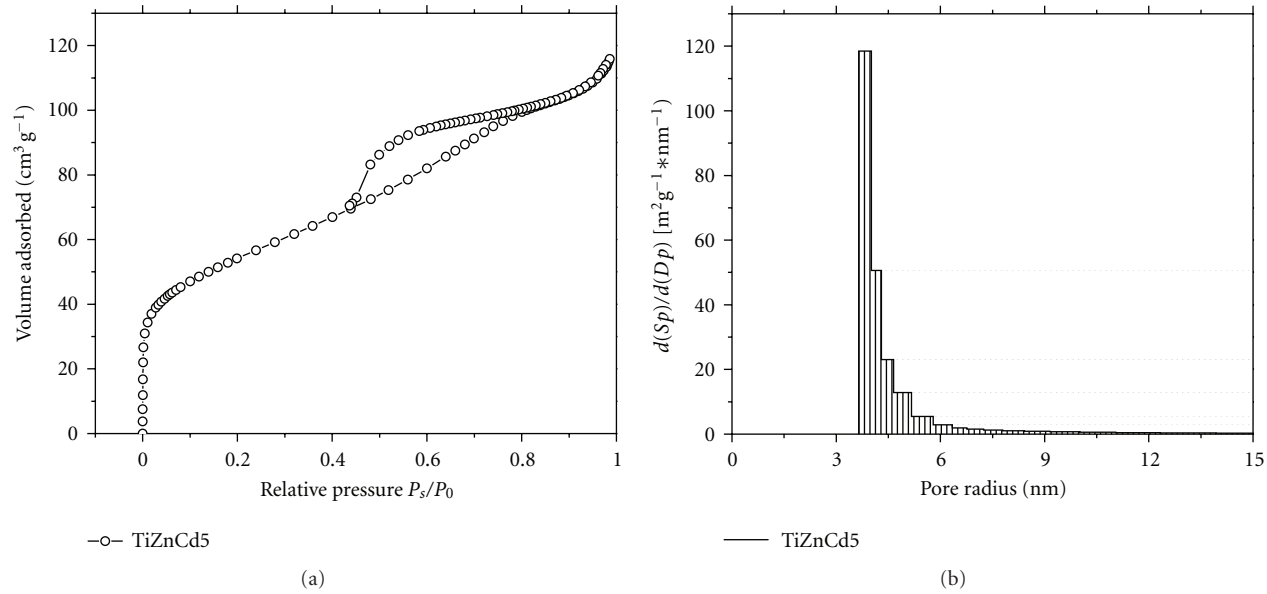

Figure 6: Hysteresis loop and pore size distribution of sample TiZnCd5.

Table 3: Surface area, porosity, and EDX analysis of nanocomposites TiO_2/ZnS/CdS.

Sample	BET surface area (m^2 g^{-1})	Total pore volume (cm^3 g^{-1})	Micropore surface area (m^2 g^{-1})	Micropore volume (cm^3 g^{-1})	EDX Ti (wt%)	EDX Zn (wt%)	EDX Cd (wt%)
TiZnCd1	133.8	0.1167	36.0	0.01539	45.06	13.33	3.15
TiZnCd2	129.9	0.0977	40.9	0.01760	51.98	5.33	4.99
TiZnCd3	94.6	0.0766	16.2	0.00627	35.81	34.46	0.55
TiZnCd4	147.8	0.1331	16.7	0.00585	46.87	12.51	0.94
TiZnCd5	193.7	0.1768	35.9	0.01482	47.40	7.33	0.69
TiZnCd6	144.8	0.1786	15.8	0.00600	29.94	42.79	0.81
TiZnCd7	106.2	0.1224	5.5	0.00146	23.25	54.73	0.75
TiZnCd8	105.6	0.1149	6.3	0.00192	28.40	43.28	1.77
TiZnCd9	107.4	0.1122	11.1	0.00408	27.15	42.19	2.22
TiZnCd10	103.8	0.0940	13.6	0.00528	19.09	10.68	47.35

The SEM micrographs of the prepared TiO_2/ZnS/CdS nanocomposites are presented in Figures 7(a)–7(j), Ti, Zn, and Cd content is presented in Table 3, as obtained from EDX analysis. The product of homogeneous precipitation of thioacetamide and zinc sulphate consists of approximately spherical round particle agglomerates of diameter about 1-2 μm (Figure 7(d)) are formed from laminar nanoparticles of size 16 nm joined to the chains [17]. The products of homogeneous hydrolysis of thioacetamide and titanium oxosulphate are 2-3 μm spherical agglomerates formed with 6 nm nanoparticles (Figure 7(i)) [15]. The TiO_2/ZnS/CdS nanocomposites are formed as mixture of single TiO_2, ZnS, and CdS agglomerates and overgrown TiO_2, ZnS, and CdS agglomerates (see Figures 7(b) and 7(h)).

The reflectance data obtained was relative percentage reflectance to a nonabsorbing material ($BaSO_4$) which can optically diffuse light. The Kubelka-Munk theory is generally used for the analysis of diffuse reflectance spectra obtained from weakly absorbing samples. It provides a correlation between reflectance and concentration. The concentration of an absorbing species can be determined using the Kubelka-Munk formula:

$$f(R) = \frac{(1-R)^2}{2R} = \frac{k}{s} = \frac{Ac}{s}, \quad (6)$$

where R is the reflectance, s is the scattering coefficient, k is the molar absorption coefficient, c is the concentration of the absorbing species, and A is absorbance [32].

Compared with the pure titania sample, obvious absorption edge red-shifts are observed in the results of the doped samples, among which the best response to visible-light is obtained in the codoped sample. The anatase has a wide absorption band in the range from 200 to 385 nm, the ZnS has an absorption band in the range from 200 to 310 nm, and CdS has absorption edge at 490 nm [33]. For the TiO_2/ZnS/CdS nanocomposites, an absorption edge red-shift is presented and the absorption tail extends to ~400 nm as Figure 8 shows. With increasing content of Cd

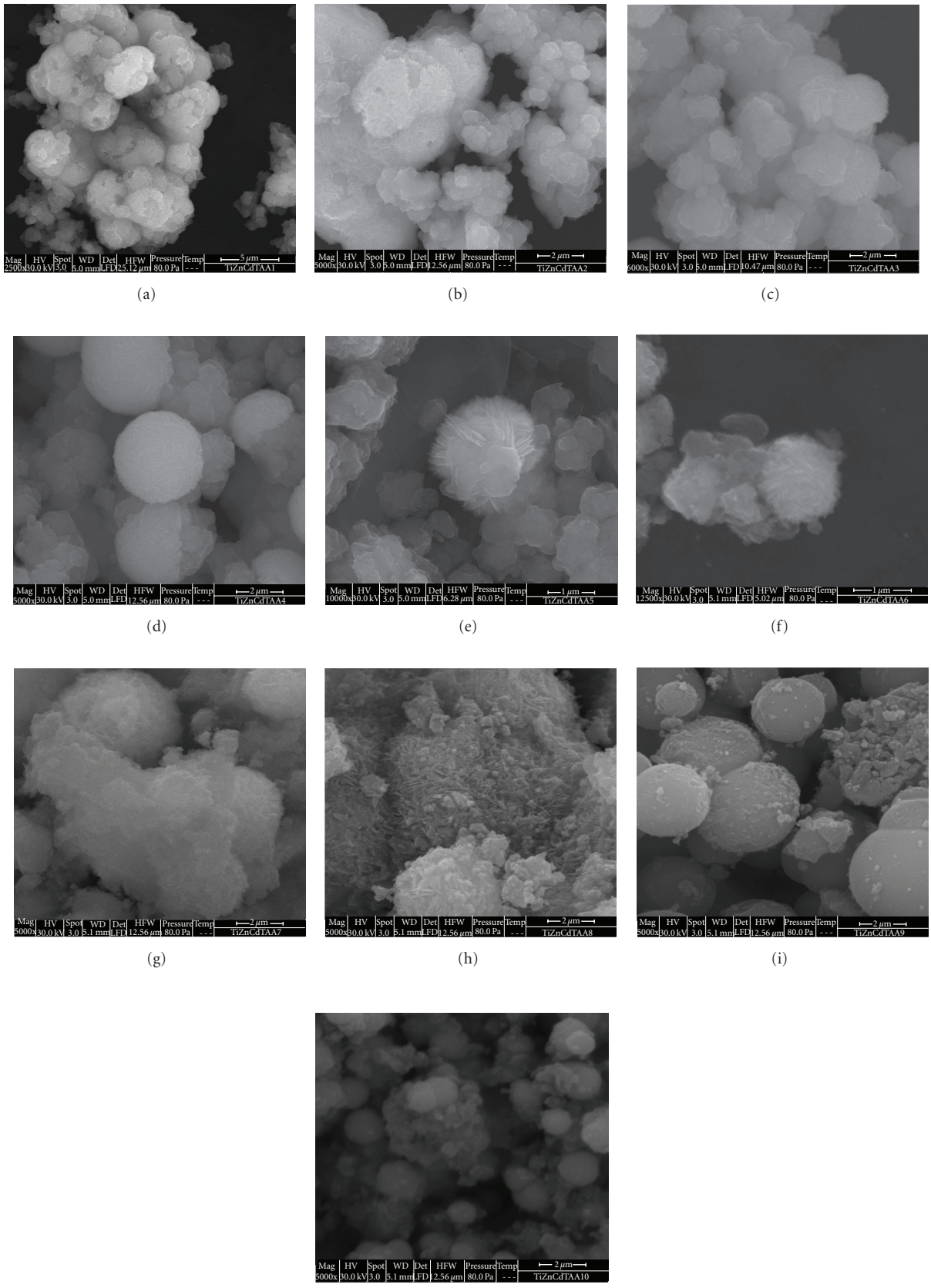

Figure 7: SEM images of sample (a) TiZnCd1, (b) TiZnCd2, (c) TiZnCd3, (d) TiZnCd4, (e) TiZnCd5, (f) TiZnCd6, (g) TiZnCd7, (h) TiZnCd8, (i) TiZnCd9, and (j) TiZnCd10.

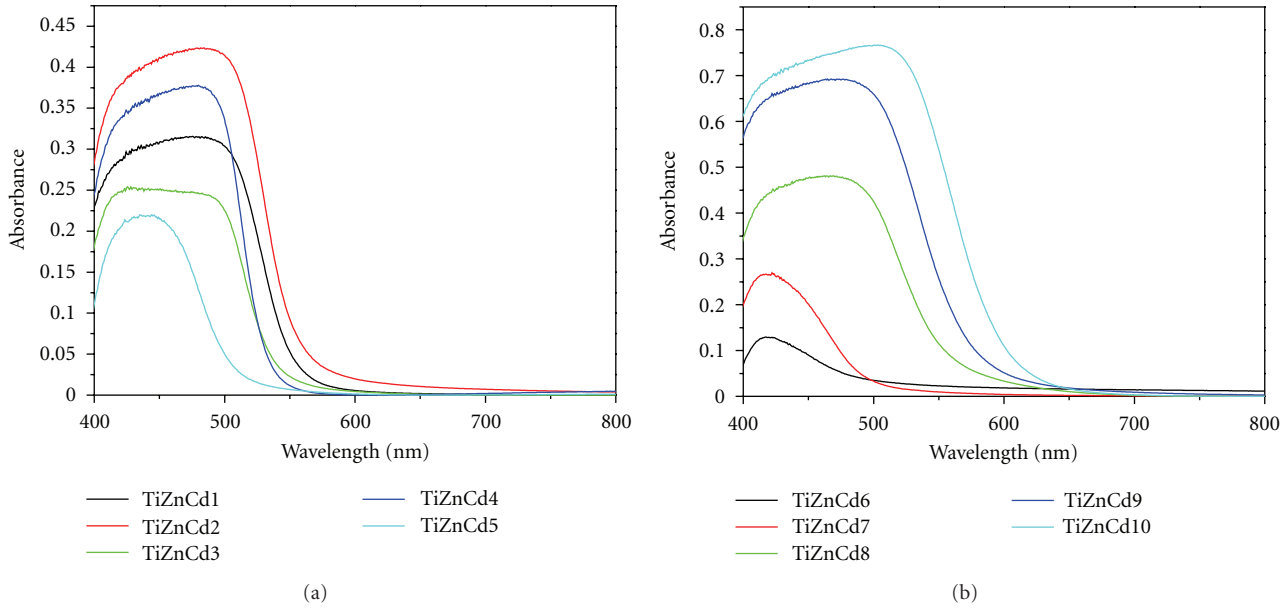

Figure 8: UV-VIS absorbance spectra of prepared TiZnCd samples.

the prepared samples are beginning to have a yellowish tinge, the sample marked TiZnCd10 is already dark orange.

The method of UV-VIS diffuse reflectance spectroscopy was employed to estimate band-gap energies of the prepared TiO_2/ZnS/CdS nanocomposites. Firstly, to establish the type of band-to-band transition in these synthesized particles, the absorption data were fitted to equations for direct band-gap transitions. The minimum wavelength required to promote an electron depends upon the band-gap energy E_{bg} of the photocatalyst and is given by

$$E_{bg} = \frac{1240}{\lambda\ (\text{eV})}, \tag{7}$$

where λ is the wavelength in nanometers [34]. The band gap values were calculated using the UV-VIS spectra from the following equation:

$$\alpha(h\nu) = A\left(h\nu - E_{bg}\right)^{n}, \tag{8}$$

where α is the absorption coefficient and $h\nu$ is the photon energy. In case the fundamental absorption of the titania crystal possesses indirect transitions between bands, then $n = 2$, for direct transition between bands $n = 1/2$ [35, 36]. The energy of the band gap is calculated by extrapolating a straight line to the abscissa axis, when α is zero, then $E_{bg} = h\nu$ [37]. Figure 9 shows the $(\alpha h\nu)^2$ versus E_{bg} for a direct band-gap transition, where α is the absorption coefficient and E_{bg} is the photon energy. The value of $h\nu$ extrapolated to $\alpha = 0$ gives an absorption energy, which corresponds to a band-gap energy (see Table 4). The value of 3.20 eV is reported in the literature for pure anatase nanoparticles [38]. ZnS has a wider energy band gap $E_{bg} = 3.7$ eV [39] than CdS has $E_{bg} = 2.4$ eV [40], which results in the transmission of more high-energy photons [41]. The value of band-gap energy decreases with increasing the content of CdS dopant.

Table 4: Rate constant of Orange II degradation and band-gap energy.

Sample	Rate constant OII 365 nm TiO_2/ZnS/CdS (min^{-1})	Rate constant OII 400 nm TiO_2/ZnS/CdS (min^{-1})	Band gap (eV)
TiZnCd1	0.01778	0.00375	2.25
TiZnCd2	0.00939	0.00251	2.20
TiZnCd3	0.00742	0.00155	2.35
TiZnCd4	0.00902	0.00248	2.35
TiZnCd5	0.03446	0.00450	2.50
TiZnCd6	0.00856	0.00271	2.65
TiZnCd7	0.00804	0.00151	2.55
TiZnCd8	0.00524	0.00132	2.20
TiZnCd9	0.00297	0.00112	2.10
TiZnCd10	0.00397	0.00078	2.05

Low values of E_{bg} in samples with higher content of CdS or ZnS may be caused by formation of sulphur compounds such as polysulphides, which were already observed in zinc sulphide or cadmium sulphide. The explanation of this effect was the agglomeration of nanoparticles [42].

The photocatalytic activity of the prepared TiO_2/ZnS/CdS nanocomposites was determined using the degradation of 0.02 M Orange II dye aqueous solutions under UV radiation at 365 nm (UV-A, black lamp). In regions in which the Lambert-Beer law is valid, the concentration of the Orange II dye is proportional to absorbance:

$$A = \varepsilon c l, \tag{9}$$

where A is absorbance, c is concentration of absorbing component, l is length of absorbing layer, and ε is molar

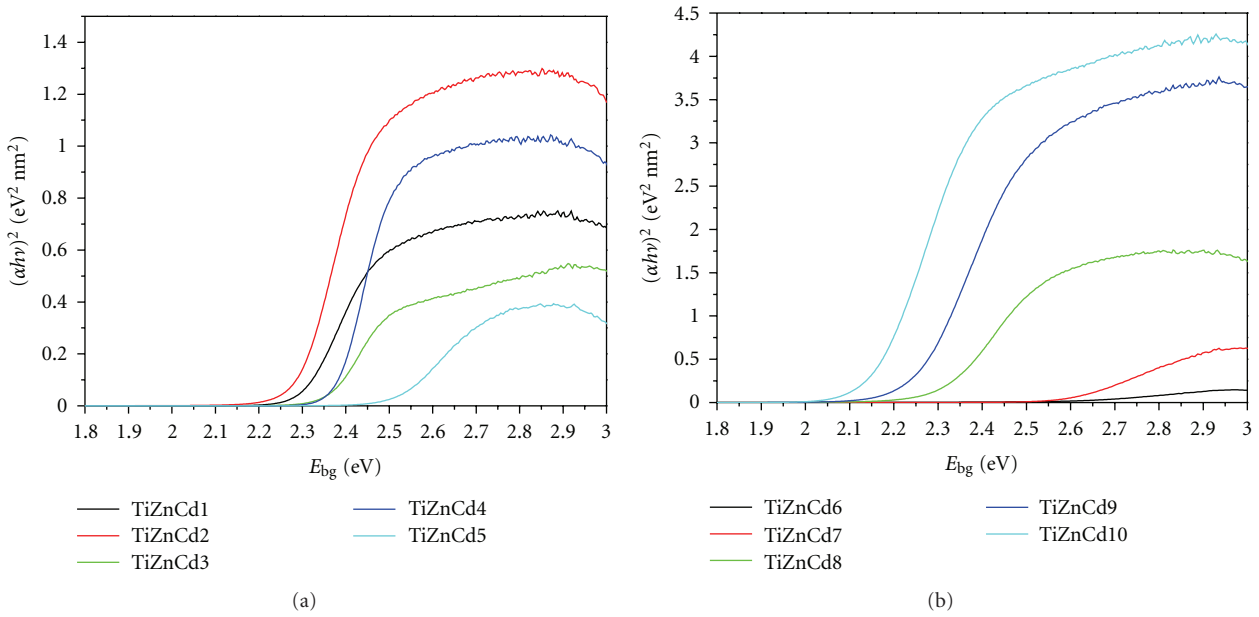

Figure 9: Band-gap energy E_{bg} of prepared TiZnCd samples.

absorbing coefficient. Orange II dye was not a subject of photolysis, and any change in Orange II dye concentration can be attributed only to the heterogeneous photocatalysis. Photodegradation experiments of Orange II dye by catalysts process exhibited first-order kinetics with respect to the concentration of the organic compound. The time dependence of Orange II dye decomposition can be described using (10) for a reaction following first-order kinetics:

$$\frac{dC}{dt} = k(C_0 - C), \tag{10}$$

where C is the concentration of Orange II dye, C_0 is the initial concentration Orange II dye, and k is the rate constant. The rate constant k of photocatalytic degradation of Orange II dye under UV and visible light are shown in Table 4 and the kinetics of the degradation are presented in Figure 10. As shown in the figure, the highest photocatalytic activity in the degradation of Orange II dye under UV and visible light have the sample labeled TiZnCd5. This seems appropriate given the high specific surface area of the sample and the highest TiO_2 content in the sample. For comparison, the rate constant for the P25 under UV is $k = 0.0471\,\text{min}^{-1}$ and under visible light is $k = 0.0022\,\text{min}^{-1}$ [43].

A heterojunction is created when two different layers of crystalline semiconductors are placed in conjunction or layered together with alternating or dissimilar band gaps. Heterojunction has been widely studied for effective decomposition of organic compounds on CdS/TiO_2 [44], $TiO_{2-x}N_x$ [45], and for photocatalytic water splitting [46]. CdS functions as a sensitizer while TiO_2 works as a substrate in the heterojunction system. When the TiO_2-CdS heterojunction was excited by UV or visible light with a photon energy higher or equal to the band gaps of TiO_2 and CdS, the electrons in the valence band could be excited to the conduction band with simultaneous generation of the same amount of holes in the valence band. In this way, the photoinduced electron-hole pairs in the two catalysts are effectively separated and the probability of electron-hole recombination is reduced. In the samples series TiO_2/ZnS/CdS highest photocatalytic activity for UV and visible light was observed in the sample denoted TiZnCd5, which is probably the optimum ratio of TiO_2 : CdS With increasing content of cadmium, too much CdS on the TiO_2 surface hinder the contact of TiO_2 with Orange II dye solution, resulting in too many electrons accumulating on the TiO_2 surface under light irradiation, leading to lower photocatalytic activity.

The sample TiZnCd5 with optimal Cd content also has the highest specific surface area (around 193 m^2) and the highest amount of anatase in the structure. Both facts contribute to significant photocatalytic activity. However, optimal cadmium content also causes beneficial activity in visible light region. With increasing amount of Cd in the structure the photoactivity decreases, as seen by samples TiZnCd9 and TiZnCd10 with lowest photocatalytic activity and high content of cadmium. These two samples have also lower specific surface area and amount of anatase, proving that both properties affect photoactivity.

The TiO_2/ZnS/CdS composites deposited on surface with Pd and Pt nanoparticles were used for hydrogen evolution from water. The hydrogen evolution on series samples TiZnCd deposited with Pd is presented in Figure 11 and samples TiZnCd deposited with Pt is presented in Figure 12. For the composites TiO_2/ZnS/CdS deposited with nano-Pt were well active only samples labeled as TiZnCd3, TiZnCd7, and TiZnCd8. The best activity for photocatalytic hydrogen evolution showed the sample marked TiZnCd7 deposited on surface with palladium.

Noble metals such as Pt, Au, and Pd have been shown to increase the photonic efficiency and inhibit electron-hole pair recombination. The optimum metal loading has major

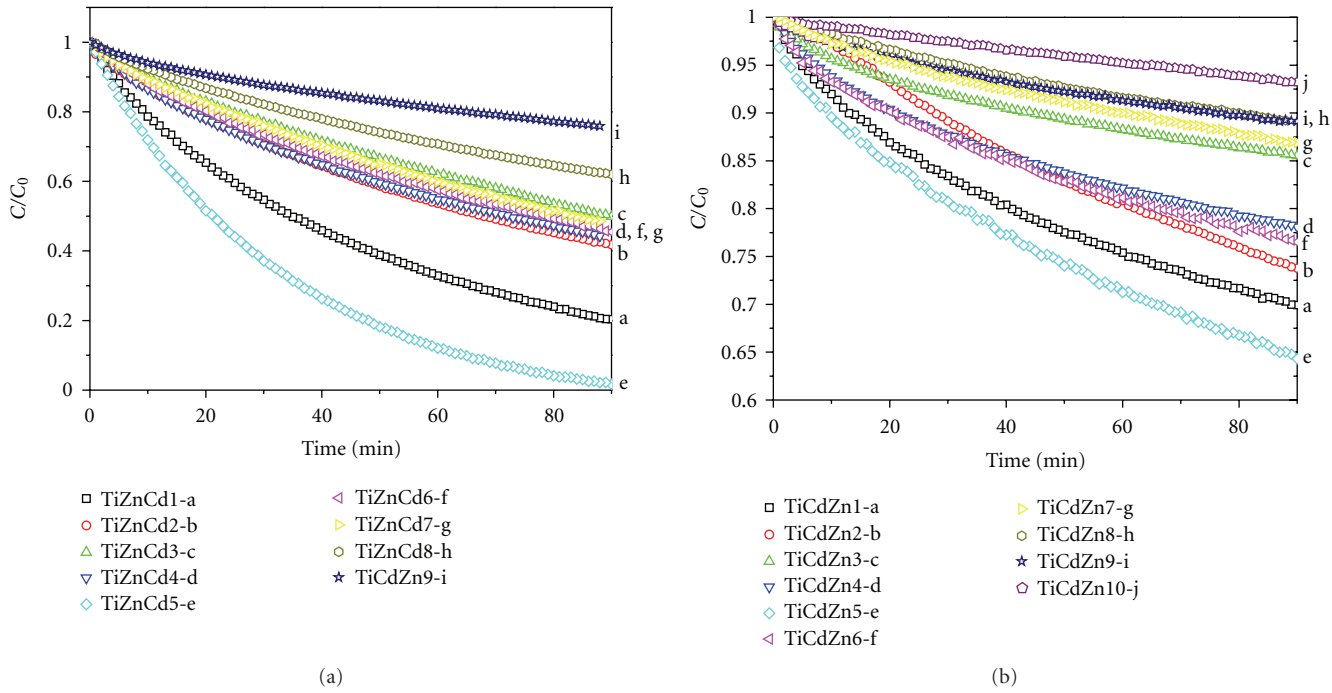

FIGURE 10: Orange II dye degradation on TiO_2/ZnS/CdS nanocomposites at wavelength of (a) 365 nm (b) over 400 nm.

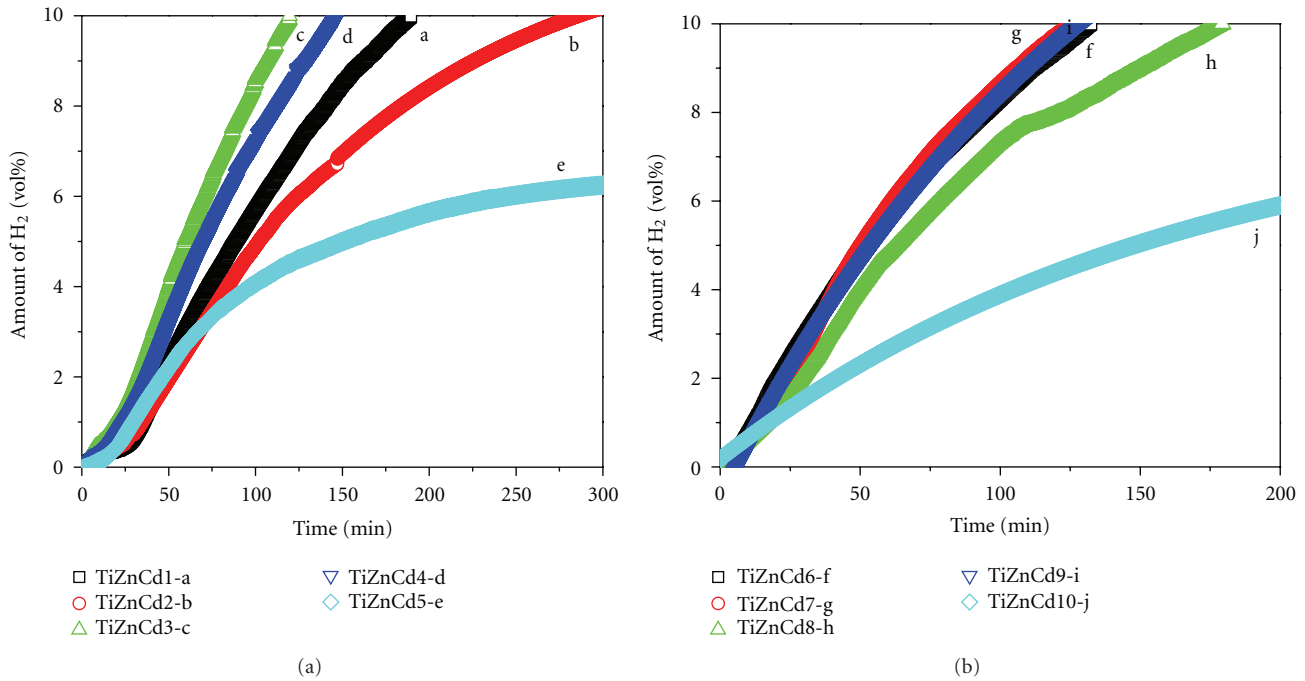

FIGURE 11: Plot of H_2 evolution on samples series TiZnCd with 1 mg Pd deposition.

role of surface deposition of small metal clusters on TiO_2 and is attributed due to the acceleration of hydroxyl radical formation and decreasing recombination which enhances the degradation rate of pollutants or active centers for hydrogen evolution. From the results [47], it is also observed that the photocatalytic efficiency increases with increase in the metal loading upto certain level (optimum metal loading) and then decreases. The excess loading of metal particles may cover active sites on the TiO_2 surface thereby reducing photodegradation efficiency.

Sadeghi et al. [48] proposed that a large number of small epitaxial deposits of noble metals on semiconductor substrate energetically capable of trapping photoelectrons may decrease charge carrier space distance and thereby

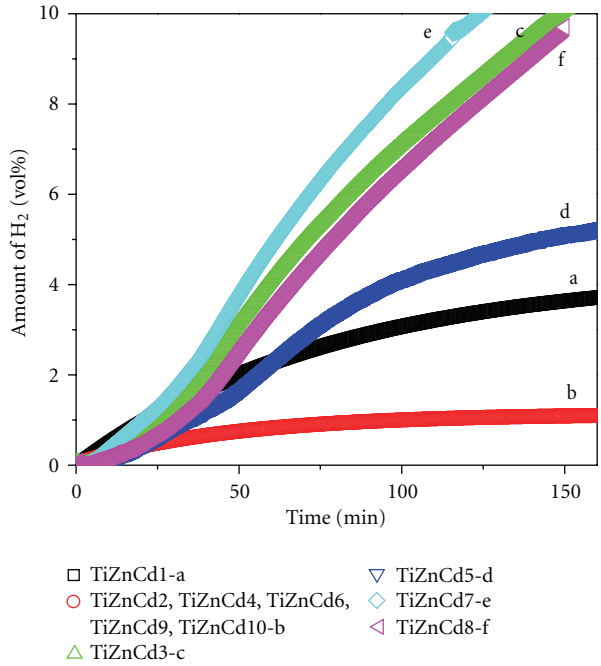

FIGURE 12: Plot of H_2 evolution on samples series TiZnCd with 1 mg Pt deposition.

increase recombination. Negative effect was observed that of photocatalytic activity when the metal loading was higher than the optimum level [49]. Excess deposition of Pt on the surface TiO_2/ZnS/CdS composite apparently causes the lower efficiency. It is observed from the experimental results that the photocatalytic efficiency for hydrogen evolution of the metal-doped TiO_2/ZnS/CdS nanocomposites is in the order Pd > Pt > Au.

Due to rapid recombination of holes h^+ and electrons e^- origins by photocatalysis, it is difficult to achieve water-splitting for hydrogen production using TiO_2 photocatalyst in distilled water. Adding electron donors or sacrificial reagents or hole scavengers to react irreversibly with the photogenerated holes h^+ can enhance the photocatalytic electron-hole separation resulting in higher quantum efficiency. Since electron donors are consumed in photocatalytic reaction, continual addition of electron donors is required to sustain hydrogen production.

One of the most well-known semiconductor photocatalyst, CdS, has been widely used for hydrogen evolution. However, pure CdS is usually not very active and prone to photocorrosion [50]. Inorganic ions such as S^{2-}/SO_3^{2-}, Ce^{4+}/Ce^{3+}, and IO^{3-}/I^- are often used as sacrificial reagents for hydrogen production. When CdS is used as photocatalyst for water-splitting hydrogen production, photocorrosion occurs as follows:

$$CdS + 2h^+ \longrightarrow Cd^{2+} + S. \quad (11)$$

Serving as a sacrificial reagent, S^{2-} can react with two holes to form S. The aqueous SO_3^{2-} ions added to reaction suspension, can dissolve S into $S_2O_3^{2-}$ in order to prevent any detrimental deposition of sulphur onto CdS. Therefore, photocorrosion of CdS is prevented. Combining CdS with the wide band-gap semiconductor ZnS to form the solid solution $Cd_{1-x}Zn_xS$ is demonstrated to be an effective way to solve the above problems. Alternative methods for improving the activity and stability of CdS include dispersion of small amounts of metal nanocrystallites (mainly Pt or Pd) on the photocatalyst surface and/or coupling with wide band-gap semiconductors with lower but closely lying conduction band level, such as TiO_2, $LaMnO_3$, and ZnS. The beneficial effect of Pd deposition on the rate of hydrogen production can be attributed to the ability of Pt or Pd crystallites to trap photogenerated electrons and to catalyze the reduction of water to hydrogen [10]. In summary, it was shown that the deposition of nano-Pd into surface of powder TiO_2/ZnS/CdS nanocomposite can be prepared photocatalysts, which could be the basis for new efficient materials for the production of hydrogen from water.

4. Conclusions

The TiO_2/ZnS/CdS nanocomposites deposited with nanoparticles of metal palladium were used for photocatalytic evolution from water. Doped titanium dioxide by the CdS reducing band-gap energy and doping with ZnS increasing photocatalytic activity. In [51] nanocomposites TiO_2/ZnS with different ZnS : TiO_2 ratios have been prepared using a chemical deposition method. The presence of small ZnS percentages on the nanocomposite surface (0.5% and 0.2%) promotes an increase in the catalyst photoactivity, when compared with the pure titania. The best photocatalytic activity for H_2 evolution shows sample named TiZnCd7 deposited with palladium, which contains 20.21% TiO_2, 78.5% ZnS, and 1.29% CdS. The TiO_2/ZnS/CdS materials have been proposed as highly efficient photocatalysts for hydrogen production, in which the location of Pd on the TiO_2/ZnS/CdS and the preparation method play an important role. The best photocatalytic activity under UV and visible light for Orange II dye degradation showed sample denoted TiZnCd5, which contains 47.4 wt% Ti, 7.33 wt% Zn, and 0.69 wt% Cd.

Acknowledgments

This work was supported by the Academy of Sciences of the Czech Republic (Project no. AV OZ 40320502) and Ministry of Industry and Trade of the Czech Republic (Project no. FT-TA5/134).

References

[1] M. Ni, M. K. H. Leung, D. Y. C. Leung, and K. Sumathy, "A review and recent developments in photocatalytic water-splitting using TiO2 for hydrogen production," *Renewable and Sustainable Energy Reviews*, vol. 11, no. 3, pp. 401–425, 2007.

[2] R. Dholam, N. Patel, M. Adami, and A. Miotello, "Physically and chemically synthesized TiO2 composite thin films for hydrogen production by photocatalytic water splitting," *International Journal of Hydrogen Energy*, vol. 33, no. 23, pp. 6896–6903, 2008.

[3] R. Dholam, N. Patel, M. Adami, and A. Miotello, "Hydrogen production by photocatalytic water-splitting using Cr- or Fe-doped TiO2 composite thin films photocatalyst," *International Journal of Hydrogen Energy*, vol. 34, no. 13, pp. 5337–5346, 2009.

[4] M. A. Khan and O. Yang, "Photocatalytic water splitting for hydrogen production under visible light on Ir and Co ionized titania nanotube," *Catalysis Today*, vol. 146, no. 1-2, pp. 177–182, 2009.

[5] M. A. Khan, S. I. Woo, and O. B. Yang, "Hydrothermally stabilized Fe(III) doped titania active under visible light for water splitting reaction," *International Journal of Hydrogen Energy*, vol. 33, no. 20, pp. 5345–5351, 2008.

[6] T. Sreethawong, C. Junbua, and S. Chavadej, "Photocatalytic H2 production from water splitting under visible light irradiation using Eosin Y-sensitized mesoporous-assembled Pt/TiO2 nanocrystal photocatalyst," *Journal of Power Sources*, vol. 190, no. 2, pp. 513–524, 2009.

[7] X. Wang, G. Liu, G. Q. Lu, and H. Cheng, "Stable photocatalytic hydrogen evolution from water over ZnO-CdS core-shell nanorods," *International Journal of Hydrogen Energy*, vol. 35, no. 15, pp. 8199–8205, 2010.

[8] S. V. Tambwekar, D. Venugopal, and M. Subrahmanyam, "H2 production of (CdS-ZnS)-TiO2 supported photocatalytic system," *International Journal of Hydrogen Energy*, vol. 24, no. 10, pp. 846–852, 1999.

[9] R. Priya and S. Kanmani, "Solar photocatalytic generation of hydrogen under ultraviolet-visible light irradiation on (CdS/ZnS)/Ag2S + (RuO2/TiO2) photocatalysts," *Bulletin of Materials Science*, vol. 1, no. 1, pp. 85–88, 2009.

[10] V. M. Daskalaki, M. Antoniadou, G. Li Puma, D. I. Kondarides, and P. Lianos, "Solar light-responsive Pt/CdS/TiO2 photocatalysts for hydrogen production and simultaneous degradation of inorganic or organic sacrificial agents in wastewater," *Environmental Science and Technology*, vol. 44, no. 19, pp. 7200–7205, 2010.

[11] V. Stengl, J. Subrt, P. Bezdicka, S. Bakardjieva, and J. Subrt, "Homogeneous precipitation with urea-an easy process for making spherical hydrous metal oxides," *Solid State Phenomena*, vol. 90-91, pp. 121–126, 2003.

[12] T. Nomura, Y. Kousaka, M. Alonso, and M. Fukunaga, "Precipitation of zinc sulfide particles from homogeneous solutions," *Journal of Colloid and Interface Science*, vol. 223, no. 2, pp. 179–184, 2000.

[13] V. Housková, V. Stengl, S. Bakardjieva, N. Murafa, A. Kalendova, and F. Oplustil, "Zinc oxide prepared by homogeneous hydrolysis with thioacetamide, its destruction of warfare agents, and photocatalytic activity," *Journal of Physical Chemistry A*, vol. 111, pp. 4215–4221, 2007.

[14] V. A. Yasir, P. N. MohanDas, and K. K. M. Yusuff, "Preparation of high surface area TiO2 (anatase) by thermal hydrolysis of titanyl sulphate solution," *International Journal of Inorganic Materials*, vol. 3, no. 7, pp. 593–596, 2001.

[15] S. Bakardjieva, V. Štengl, J. Šubrt, M. J. Dianez, and M. J. Sayagues, "Photoactivity of anatase-rutile TiO2 nanocrystalline mixtures obtained by heat treatment of homogeneously precipitated anatase," *Applied Catalysis B*, vol. 58, no. 3-4, pp. 193–202, 2005.

[16] L. J. Zhang, X. C. Shen, H. Liang, S. Guo, and Z. H. Liang, "Hot-injection synthesis of highly luminescent and monodisperse CdS nanocrystals using thioacetamide and cadmium source with proper reactivity," *Journal of Colloid and Interface Science*, vol. 15, no. 2, pp. 236–242, 2010.

[17] V. Housková, V. Stengl, S. Bakardjieva, N. Murafa, K. Kalendova, and F. Oplustil, "Nanostructure materials for destruction of warfare agents and eco-toxins prepared by homogeneous hydrolysis with thioacetamide: part 1-zinc oxide," *Journal of Physics and Chemistry of Solids*, vol. 68, pp. 716–720, 2007.

[18] JCPDS PDF-2 database, International Centre for Diffraction Data, Newtown Square, Pa, U.S.A. Release 54, 2004.

[19] ICSD database FIZ Karlsruhe, Germany, release 2009/1, 2009.

[20] S. Brunauer, P. H. Emmett, and E. Teller, "Adsorption of gases in multimolecular layers," *Journal of the American Chemical Society*, vol. 60, no. 2, pp. 309–319, 1938.

[21] E. P. Barrett, L. G. Joyner, and P. P. Halenda, "The determination of pore volume and area distributions in porous substances. I. computations from nitrogen isotherms," *Journal of the American Chemical Society*, vol. 73, no. 1, pp. 373–380, 1951.

[22] Z. C. Orel, M. K. Gunde, and B. Orel, "Application of the Kubelka-Munk theory for the determination of the optical properties of solar absorbing paints," *Progress in Organic Coatings*, vol. 30, no. 1-2, pp. 59–66, 1997.

[23] H. Lachheb, E. Puzenat, A. Houas et al., "Photocatalytic degradation of various types of dyes (Alizarin S, Crocein Orange G, Methyl Red, Congo Red, Methylene Blue) in water by UV-irradiated titania," *Applied Catalysis B*, vol. 39, no. 1, pp. 75–90, 2002.

[24] J. M. Monteagudo and A. Durán, "Fresnel lens to concentrate solar energy for the photocatalytic decoloration and mineralization of orange II in aqueous solution," *Chemosphere*, vol. 65, no. 7, pp. 1242–1248, 2006.

[25] V. Štengl, V. Houšková, S. Bakardjieva, N. Murafa, and V. Havlín, "Optically transparent titanium dioxide particles incorporated in poly(hydroxyethyl methacrylate) thin layers," *Journal of Physical Chemistry C*, vol. 112, no. 50, pp. 19979–19985, 2008.

[26] P. Scherrer, "Bestimmung der Größe und der inneren struktur von kolloidteilchen mittels röntgenstrahlen. Nachrichten von der gesellschaft der wissenschaften zu göttingen," *Mathematisch-Physikalische Klasse*, vol. 2, p. 98, 1918.

[27] S. Kaneko, H. Aoki, Y. Kawahara, and F. Imoto, "Solid solutions and phase transformations in the system ZnS-CdS under hydrothermal conditions," *Journal of The Electrochemical Society*, vol. 131, pp. 1445–1446, 1984.

[28] V. A. Fedorov, V. A. Ganshin, and Y. N. Korkishko, "Solid-state phase diagram of the zinc sulfide-cadmium sulfide system," *Materials Research Bulletin*, vol. 28, no. 1, pp. 59–66, 1993.

[29] W. Li, D. Li, W. Zhang, Y. Hu, Y. He, and X. Fu, "Microwave synthesis of ZnxCd1-xS nanorods and their photocatalytic activity under visible light," *Journal of Physical Chemistry C*, vol. 114, no. 5, pp. 2154–2159, 2010.

[30] S. Arora and S. S. Manoharan, "Tuning of Mn(II)-doped CdS—ZnS solid solutions for broadband emission," *Materials Chemistry and Physics*, vol. 110, no. 1, pp. 34–37, 2008.

[31] J. A. de Boer, *In Structure & Properties of Porous Materials*, Academic Press, 1958.

[32] A. A. Christy, O. M. Kvalheim, and R. A. Velapoldi, "Quantitative analysis in diffuse reflectance spectrometry: a modified Kubelka-Munk equation," *Vibrational Spectroscopy*, vol. 9, no. 1, pp. 19–27, 1995.

[33] H. Yin, Y. Wada, T. Kitamura, and S. Yanagida, "Photoreductive dehalogenation of halogenated benzene derivatives using ZnS or CdS nanocrystallites as photocatalysts," *Environmental Science and Technology*, vol. 35, no. 1, pp. 227–231, 2001.

[34] K. M. Reddy, S. V. Manorama, and A. R. Reddy, "Bandgap studies on anatase titanium dioxide nanoparticles," *Materials Chemistry and Physics*, vol. 78, no. 1, pp. 239–245, 2002.

[35] D. R. Coronado, G. R. Gattorno, M. E. E. Pesqueira, C. Cab, R. de Coss, and G. Oskam, "Phase-pure TiO2 nanoparticles: anatase, brookite and rutile," *Nanotechnology*, vol. 19, no. 14, Article ID 145605, p. 10, 2008.

[36] N. Serpone, D. Lawless, and R. Khairutdinov, "Size effects on the photophysical properties of colloidal anatase TiO2 particles: size quantization or direct transitions in this indirect semiconductor?" *Journal of Physical Chemistry*, vol. 99, no. 45, pp. 16646–16654, 1995.

[37] E. Sanchez and T. Lopez, "Effect of the preparation method on the band gap of titania and platinum-titania sol-gel materials," *Materials Letters*, vol. 25, no. 5-6, pp. 271–275, 1995.

[38] D. S. Bhatkhande, V. G. Pangarkar, and A. A. Beenackers, "Photocatalytic degradation for environmental applications—a review," *Journal of Chemical Technology and Biotechnology*, vol. 77, no. 1, pp. 102–116, 2001.

[39] M. Y. Nadeem and W. Ahmed, "Optical properties of ZnS thin films," *Turkish Journal of Physics*, vol. 24, no. 5, pp. 651–659, 2000.

[40] D. Patidar, R. Sharma, N. Jain, T. P. Sharma, and N. S. Saxena, "Optical properties of CdS sintered film," *Bulletin of Material Science*, vol. 29, pp. 21–24, 2006.

[41] A. Henglein, "Catalysis of photochemical reactions by coloidal semiconductors," *Pure and Applied Chemistry*, vol. 56, no. 9, pp. 1215–1224, 1984.

[42] R. Künneth, G. Twardzik, G. Emig, and H. Kisch, "Heterogeneous photocatalysis XI. Zinc sulphide catalysed dehydrodimerization of dihydropyrans and cyclohexene," *Journal of Photochemistry and Photobiology, A*, vol. 76, no. 3, pp. 209–215, 1993.

[43] V. Štengl, S. Bakardjieva, and N. Murafa, "Preparation and photocatalytic activity of rare earth doped TiO2 nanoparticles," *Materials Chemistry and Physics*, vol. 114, no. 1, pp. 217–226, 2009.

[44] S. Shen, L. Guo, X. Chen, F. Ren, C. X. Kronawitter, and S. S. Mao, "Effect of noble metal in CdS/M/TiO2 for photocatalytic degradation of methylene blue under visible light," *International Journal of Green Nanotechnology: Materials Science & Engineering*, vol. 1, pp. 94–104, 2010.

[45] V. Etacheri, M. K. Seery, S. J. Hinder, and S. C. Pillai, "Highly visible light active TiO2-xNx heterojunction photocatalysts," *Chemistry of Materials*, vol. 22, pp. 3843–3853, 2010.

[46] H. Park, W. Choi, and M. R. Hoffmann, "Effects of the preparation method of the ternary CdS/TiO2/Pt hybrid photocatalysts on visible light-induced hydrogen production," *Journal of Materials Chemistry*, vol. 18, no. 20, pp. 2379–2385, 2008.

[47] S. Sakthivel, M. V. Shankar, M. Palanichamy, B. Arabindoo, D. W. Bahnemann, and V. Murugesan, "Enhancement of photocatalytic activity by metal deposition: characterisation and photonic efficiency of Pt, Au and Pd deposited on TiO2 catalyst," *Water Research*, vol. 38, no. 13, pp. 3001–3008, 2004.

[48] M. Sadeghi, W. Liu, T. G. Zhong, P. Stavropoulos, and B. Levy, "Role of photoinduced charge carrier separation distancein heterogeneous photocatalysis oxidative degradation of CH3OH vapour in contact with Pt-TiO2 and confirmedTiO2-Fe2O3," *Journal of Materials Chemistry*, vol. 100, pp. 19466–19474, 1996.

[49] M. D. Driessen and R. H. Grassian, "Photooxidation of trichloroethylene on Pt/TiO2," *Journal of Physical Chemistry B*, vol. 102, no. 8, pp. 1418–1423, 1998.

[50] K. Zhang, D. Jing, C. Xing, and L. Guo, "Significantly improved photocatalytic hydrogen production activity over Cd1-xZnxS photocatalysts prepared by a novel thermal sulfuration method," *International Journal of Hydrogen Energy*, vol. 32, no. 18, pp. 4685–4691, 2007.

[51] A. Franco, M. C. Neves, M. M. L. R. Carrott, M. H. Mendonça, M. I. Pereira, and O. C. Monteiro, "Photocatalytic decolorization of methylene blue in the presence of TiO2/ZnS nanocomposites," *Journal of Hazardous Materials*, vol. 161, no. 1, pp. 545–550, 2009.